Apparatus for Dry Deposition of Aerosols on Snow

Nicholas D. Beres[1,2] and Hans Moosmüller[1]

[1]Laboratory for Aerosol Science, Spectroscopy, and Optics, Desert Research Institute, Reno, NV, 89512, United States
[2]University of Nevada-Reno, Reno, NV, 89512, United States

Correspondence to: Nicholas D. Beres (Nic.Beres@DRI.edu)

Abstract. Deposition of light absorbing aerosol on snow can drastically change the albedo of the snow surface and the energy balance of the snowpack. To study these important effects experimentally and to compare with theory, it is desirable to have an apparatus for such deposition experiments. Here, we describe a simple apparatus to generate and evenly deposit light absorbing aerosols onto a flat snow surface. Aerosols are produced (combustion aerosols) or entrained (mineral dust aerosols) and continuously transported into a deposition chamber placed on the snow surface where they deposit onto and into the snowpack, thereby modifying its surface reflectance and albedo. We demonstrate field operation of this apparatus by generating black and brown carbon combustion aerosols and entraining hematite mineral dust aerosol and depositing them on the snowpack. Changes in spectral snow reflectance is demonstrated qualitatively through pictures of snow surfaces after aerosol deposition and quantitatively by measuring hemispherical-conical reflectance spectra for the deposited areas and for adjacent snowpack in its natural state. Additional potential applications for this apparatus are mentioned and briefly discussed.

1 Introduction

Aerosols in the Earth-atmosphere system play a critical role in radiative forcing and climate change (IPCC, 2013). However, our understanding of how they affect the cryosphere upon deposition onto snow surfaces is still limited (Qian et al., 2015). Understanding aerosol-cryosphere interactions is important on several levels, including: (1) the radiative properties of the snowpack modified by deposited aerosols (Warren and Wiscombe, 1980; Warren 1982; Gardner and Sharp, 2010; Bond et al., 2013; Qian et al., 2015), which alter the seasonal timing of snow melt, runoff, and water management (Painter et al., 2010; Dozer, 2011), (2) the relation between deposited nutrients and the snowpack biosphere (Thomas and Duval, 1995; Jones, 1999; Kuhn, 2001; Hodson et al., 2008), and (3) snowpack chemistry and photochemistry, which are influenced by the deposited chemical compounds and their interaction with solar radiation (Grannas et al, 2007). One limitation in our understanding is establishing links between theoretical and experimental results because it is difficult to experimentally characterize these interactions in a controlled manner; generally, aerosol deposition on snow is spatially and temporally very inhomogeneous, and often deposition and its immediate effects are minor. One scarcely-used but effective experimental method is to artificially deposit aerosols of interest directly onto the snow surface.

Atmospheric deposition is an important process by which an exchange of nutrients, gasses, and particles takes place between the atmosphere and land and sea surfaces. Many deposition processes are irreversible; for example, once the deposition of particles occurs, the probability of re-entrainment is low. Atmospheric constituents are removed from the atmosphere through dry and wet deposition (Seinfeld and Pandis, 2016). Dry deposition is facilitated by gravitational settling, inertial impaction, and Brownian diffusion processes. Wet deposition, on the other hand, involves the scavenging of gasses and particles by clouds and precipitation through dissolution, CCN activity, and collision processes. For snowpack radiative processes and energy balance, the deposition of light absorbing aerosols (i.e., black carbon (BC), brown carbon (BrC), and mineral dust, Moosmüller et al., 2009) is of special interest because deposition of even minute quantities of strongly light-absorbing aerosols drastically increases the co-albedo of the snow surface in the visible and near-visible spectral regions, where pure snow is "snow-white" with hardly any intrinsic absorption (Warren, 1982).

Carbonaceous aerosols in the atmosphere, including BC and BrC (Chakrabarty et al., 2010; Lack et al., 2014), are dominantly generated by incomplete combustion of fossil and biomass fuels with significant additional generation of secondary

organic aerosols through oxidation of volatile precursors in the atmosphere (Bond et al., 2004; Lin et al., 2014). These aerosols are lofted into the atmosphere, where, during transport of a few days to weeks, they undergo secondary processing (Jimenez et al., 2009) and eventually are removed from the atmosphere through wet or dry deposition (Bond et al., 2013). BC is a ubiquitous light-absorbing aerosol in the atmosphere that directly affects Earth's radiative budget (Jacobson, 2001; Bond et al., 2013) and the cryosphere (Hegg et al., 2009; Flanner et al., 2009; Hadley and Kirchstetter, 2012; Qian et al., 2015). Recently, BrC has become of interest regarding its role in atmospheric light absorption (Laskin et al., 2015) and even more recently a topic of concern for affecting snow albedo and energy balance (Dang and Hegg, 2014; Doherty et al., 2014; Lin et al., 2014; Wu et al., 2016). The fraction of BC versus BrC mass emitted by combustion sources depends greatly on a number of factors, including fuel type, fuel moisture content, and packing density (Sumlin et al., 2018), combustion phase (Patterson and McMahon, 1984; Reid et al., 2004; Bond et al., 2004), and other elements of the system (Chen and Moosmüller, 2006). For BC, the imaginary part κ of the refractive index is relatively large ($\kappa \approx 0.79$) and varies little over the visible and near-visible wavelength regions (Bond et al., 2006; Moosmüller et al., 2009). Because the imaginary part of the refractive index is so high for BC relative to that of snow, a small amount of BC present in the snowpack significantly increases the co-albedo in those spectral regions (Warren and Wiscombe, 1980; Cereceda-Balic et al., 2018). For BrC, the imaginary part of the refractive index generally increases towards shorter visible and ultra-violet wavelengths (Chakrabarty et al., 2010; Moosmüller et al, 2009; Moosmüller et al., 2011). Combustion systems – typically smoldering wildland fires – that produce a significant amount of BrC will have smoke plumes that are brownish or yellowish in appearance because of this spectral dependence (Andreae and Gelencsér, 2006). For this study, the boreal peat fuel used is the same as used by Sumlin et al. (2018), who found a value of $\kappa = 0.014$ at 375 nm, $\kappa = 0.003$ at 532 nm, and $\kappa = 0.002$ at 1047 nm. We are not aware of any published studies that explore the impact of deposition from a BrC dominated emission source on snow or identify the spectral reflectance signature of BrC particles deposited onto snow.

In addition to the importance of carbonaceous aerosol deposition on snow, mineral dust deposition has been shown to be an important driver of early snowmelt in some mountains (e.g., Painter et al., 2007; Skiles et al., 2012; Painter et al., 2012; Painter et al., 2017). The light absorption of mineral dust is mostly caused by iron oxides, such as hematite (Fe_2O_3) (Moosmüller et al., 2012; Zhang et al., 2015; Engelbrecht et al., 2016). Hematite is a mineral dust component with global-scale abundance and has been found to significantly absorb light in the ultra-violet and visible wavelengths - the imaginary refractive index of hematite is larger the shorter visible wavelengths and near UV ($\kappa \approx 0.90$ at 460 nm) and decreases with increasing wavelength (e.g., $\kappa \approx 0.035$ at 2500 nm) (Querry, 1985; Moosmüller et al, 2009; Dubovik et al, 2002) - and may have the largest optically absorptive impact of all mineral dust components found in the cryosphere (Hegg et al, 2010). Mineral dust deposition on snow is a major concern for the albedo feedback effects in certain areas of the cryosphere (McConnell et al., 2007; Painter et al., 2007; Skiles et al., 2012; Zhou et al., 2017), and accurate experimental representation of dust depositions is critical to understanding their interaction with snow.

Previous experiments have utilized aerosol artificial deposition techniques to test non-natural snow surface albedo perturbations, but with varying success. Brandt et al. (2011) measured the snow albedo resulting from mixing commercially-available soot into tap water and spraying the mixture through a commercially-available snow-making machine over a field of artificial snowpack, produced with the same means. More recently, Peltoniemi et al. (2015) distributed chimney soot, glaciated silt, and volcanic sand onto the snow surface using a "salt shaker" in an attempt to measure the bidirectional reflectance factor of the resulting, contaminated snow. In addition, the snow albedo response to absorbing impurities on snow has been characterized by Singh et al. (2010) "spraying…soil equally on the surface".

Our work presented here describes a simple apparatus to evenly deposit aerosols in an artificial manner onto a flat snow surface through dry deposition for the study of snow-aerosol interactions. Tests over the 2015-2016 and 2016-2017 snow seasons were conducted at the Cold Regions Research and Engineering Laboratory/UC Santa Barbara Energy Site (CUES, Bair et al, 2015) on Mammoth Mountain, California, USA and in the Carson Range of the Sierra Nevada Mountains in Nevada, USA, respectively. Controlled deposition experiments using the apparatus for hematite mineral dust entrainment and combustion aerosol production of BC and BrC to modify snow surface reflectance are presented as examples.

2 Description and Operation of Apparatus

The deposition apparatus presented here is composed of two primary components: the aerosol production or entrainment chamber and the deposition chamber. The materials used for the air source and production or entrainment chamber depend on the type of test aerosol generated or entrained and deposited onto the snow surface. The deposition chamber is the same for any type of aerosol used.

2.1 Aerosol Production Chamber (Combustion Aerosols)

A schematic diagram of the aerosol production chamber for generating combustion aerosols is shown in Figure 1. It consists of a flat plywood base with an area of ~0.5 m^2 and a ~10 L near-cylindrical galvanized steel volume fitted with a ~1 L volume cone to its top; the cone funnels aerosols towards the chamber outlet. Inside of the chamber, a ~6 cm high stage is mounted on the plywood base, directly above a perforated inlet that disperses inlet air horizontally under the combustion stage. The bottom rim of the chamber is lined with a rubber seal that, when mounted to the plywood base with clamps, becomes near-airtight. The combustion stage can be adapted to house different combusting configurations to fit the user's needs; generally, it symmetrically distributes inlet air around the stage and serves as platform for fuels to be burned. The air source used in the combustion aerosol configuration has three purposes: (1) to provide the appropriate amount of air for (incomplete) combustion to take place, (2) to provide continuous flow to move the combustion aerosols vertically (with assistance from flame buoyancy) through the production chamber towards the outlet, and to create a pressure differential between the production chamber and the deposition chamber that ultimately moves aerosols from the production chamber to the deposition chamber and finally onto and into the snowpack. If the heat from the combustion source is too intense, a small amount of metal tubing arranged in a coil may be necessary to cool the combustion air before being transported through any conducting rubber tubing, as shown in Figure 3.

The air source used for this configuration is a battery-powered, 12-volt air pump that provides inlet air into the entrainment chamber, with a flow rate of ~5.3 LPM at the outlet of the production chamber. This outlet is connected to the deposition chamber mostly via 6 mm OD copper tubing, as rubber or plastic tubing near the production chamber may melt from the combustion heat.

The user of this apparatus can vary the mass of combustion material deposited by limiting the amount of time the fuel is combusting. Here, we purposefully produced heavy depositions for optical inspection and verification of the proper operation of the apparatus.

2.1.2 Aerosol Entrainment Chamber (Mineral Dust Aerosols)

For pulverized, dry solids such as mineral dusts, the entrainment chamber consists of a 1 L volume glass Büchner flask (e.g., Jensen, 2006), but used in an opposing manner, providing positive pressure rather than a vacuum. Here, the flask is filled with a generous amount (~90 g) of the dust of interest, changing this amount allows for controlling the dust mass deposited onto the snow in the deposition chamber. Compressed air is introduced into the flask through the large opening at its top, sealed with a rubber stopper. The flask's short, horizontal tube acts as the outlet for entrained aerosols and is connected directly to the deposition chamber via conductive tubing. Dry solids are adequately re-suspended using short, intense bursts of air typically between 200 and 300 kPa in pressure from a hand-operated, positive-displacement piston pump, such as a common bike floor pump. A similar setup for the entrainment of mineral dust has previously been used by Moosmüller et al. (2012), Engelbrecht et al. (2016), and Piedra et al. (2018).

2.2 Deposition Chamber

The deposition chamber for all aerosols is a near-cylindrical galvanized steel volume that measures approximately 50 cm in diameter at its midpoint and has a volume of ~100 L. This piece of the apparatus is shown in Figure 2. There is an inlet at the top of the volume that allows for aerosol flow from the production or entrainment chamber and disperses the aerosols into the volume by splitting the aerosol flow into three separate outflows symmetrical about the center of the chamber, for uniform aerosol deposition onto the snow surface.

3 Characterization of Apparatus and Results

To demonstrate the effectiveness of this deposition apparatus, it was tested during the spring of the 2016, 2017, and 2018. Deposition of three different aerosol types was demonstrated: BC and BrC in the combustion aerosol production configuration and a dry, sieved mineral dust, hematite (Fe_2O3), to test the entrainment configuration. Hematite deposition was tested at the Cold Regions Research and Engineering Laboratory/UC Santa Barbara Energy Site (CUES, Bair et al, 2015) on Mammoth Mountain, California (39° 38' 34.8" N, 119° 1' 44.3994" W, 2940 masl) on 11 May 2016. BrC and BC deposition was tested in the Carson Range of the Sierra Nevada Mountains at Tamarack Lake, NV (39° 19' 2.517" N, 119° 54' 19.512" W, 2694 masl) on 02 May 2017 and 24 April 2018, respectively; the lake was frozen and covered by snow deposited on its ice surface, creating a flat, homogeneous natural snowpack that is ideal for testing this apparatus.

To quantify the effect of aerosol deposition onto a natural snow surface, both subjective and objective measures were used. The uniformity of the aerosol deposition was inspected visually for aerosol types that are visually dark, or optically absorbing, as for the hematite deposition in Figure 4. In addition, the hemispherical-conical reflectance factor (HCRF, Schaepman-Strub et al., 2006) was measured with an Analytical Spectral Devices (ASD) FieldSpec3 spectroradiometer to verify that aerosol was indeed altering the surface spectral reflectivity of the snow and to spectrally quantify that effect. Note, that the measured HCRF is related to the surface albedo, controlling solar energy input to the snowpack (Schaepman-Strub et al., 2006). After deposition of the different aerosol species, HCRF was measured for the deposition area as well as for an adjacent, untreated, natural surface that mirrored the snow properties of the deposition area prior to deposition. This allowed the characterization and verification of the snow reflectivity reduction due to aerosol deposition. Ten measurements of HCRF were performed and averaged for each deposition area. This averaged value is presented throughout this paper with one standard deviation of the mean.

Measurement information and environmental conditions are summarized in Table 1. Solar zenith angles have been obtained from the date and time of the measurement using the NOAA ESRL Solar Position Calculator (https://www.esrl.noaa.gov/gmd/grad/solcalc/azel.html). The spectrometer optical input is a nadir-viewing cone with full angle of 25°. Meteorological information was obtained for the Tamarack Lake site from the nearby NRCS SNOTEL site at Mt Rose (2683 masl, https://wcc.sc.egov.usda.gov/nwcc/site?sitenum=652) and for the CUES site from its meteorological instrumentation (http://snow.ucsb.edu/).

3.1 Example: Combustion Aerosol Deposition

3.1.1 Black Carbon (BC) Deposition

Generation and deposition of BC aerosol took place during the spring of 2018 at Tamarack Lake. A kerosene lamp was used to produce BC aerosol (Arnott et al., 2000; Arnold et al., 2014) to be deposited onto the snow surface. First, the 12-volt pump was started to begin moving air through the complete apparatus and provide enough air to sustain the combustion; without this forced air, the flame would quickly be extinguished due to lack of oxidant. The kerosene lamp was filled with fuel and lit before being placed onto the combustion stage and the production chamber being sealed with clamps. Then, the deposition chamber was lowered onto the desired snow surface, thereby initiating BC deposition on the snow. For this experiment, the kerosene lamp was ignited, and aerosol emissions were pumped into the deposition chamber for 45 minutes. After this time, the flame was extinguished manually, and air was pumped through the apparatus for an additional 15 minutes to facilitate further deposition of aerosol onto and into the snowpack. The deposition chamber was promptly removed and spectral reflection properties of the deposited and nearby undeposited snow surfaces were characterized with HCRF measurements.

This deposition of BC aerosol reduced the HCRF from ~0.87 ± 0.003 to ~0.58 ± 0.006 at 500 nm, an approximate reduction of ~33% corresponding to a large increase (~factor of 3) of the solar energy input to the snowpack. An image of the deposition area is presented in Figure 5 along with corresponding HRCF measurements made for the deposition area and for adjacent natural snow. Of the example depositions presented, this deposition was the least uniform.

3.1.2 Brown Carbon (BrC) Deposition

The fuel combusted for BrC aerosol generation consisted of boreal peat samples collected from interior Alaska, USA. Details of this fuel – including its collection and preparation – have been given by Chakrabarty et al. (2016). The optical, physical, and chemical properties of aerosol emissions from combustion of this fuel have been extensively studied to evaluate the impact

5 of its combustion emissions on air quality and radiative forcing in the atmosphere through optical, physical, and chemical characterization (Chakrabarty et al., 2016; Samburova et al., 2016; Sengupta et al., 2018; Sumlin et al., 2017; Sumlin et al., 2018). Prior to combustion, the fuel samples were placed into a round, insulated container to mimic simple, real-world conditions in which there is little lateral heat flux due to largely homogeneous horizontal conditions. The fuel samples were burning with nearly exclusively smoldering phase combustion, producing OC-rich biomass burning aerosols. The fuel samples

10 were smoldering for ~30-40 minutes; after this period, we continued to pump air through the apparatus for an additional 15 minutes to facilitate further deposition of aerosol onto and into the snowpack. Following the deposition, the deposition chamber was removed and HCRF measurements were made on the deposited and nearby undisturbed snow surfaces.

BrC deposited onto the snow surface greatly reduced the measured HCRF, but only at the shorter visible and UV wavelengths. The effect presented here reduced the reflectivity of a springtime snowpack from 0.92 ± 0.003 for the adjacent

15 natural snowpack to 0.53 ± 0.02 at 350 nm, a reduction of ~39% for the BrC deposited snow. The resulting image and spectrum are presented in Figure 6. The image of the deposition clearly shows a yellowish appearance, an indication of BrC's preferential absorption of blue wavelengths. This visual impression and the corresponding spectrum (Figure 6), confirms the dominance of BrC over BC aerosol within the snowpack, as BC would have reduced snow reflectivity across the visible and near-visible spectrum and resulted in a greyish or blackish appearance on the snow surface.

20 ### 3.2 Example: Deposition of Resuspended Mineral Dust - Hematite

Mineral dust in the atmosphere – and that deposited into the cryosphere – has varying optical properties depending on its chemical and mineralogical composition. Here, synthetically-made, pure hematite (Fe_2O_3) was used as surrogate for strongly absorbing, red-coloured mineral dust with high iron-oxide and hematite content. Depositions of hematite were made on a relatively level, undisturbed snow surface at the CUES research site.

25 A generous amount – approximately 90 g – of hematite dust was placed into the Büchner flask and was entrained and pumped into the deposition chamber as described in Section 2. The dust was allowed to gravitationally settle onto the snow surface for approximately 30 minutes, at which time the deposition chamber was removed and HCRF measurements were made for the deposited snow surface and the adjacent natural snow. The resulting image and spectrum from this test are shown in Figure 7. The resulting HCRF was reduced by approximately 35% in the 350 – 575 wavelength range when compared to

30 that of the nearby natural snowpack.

3.4 Challenges and Further Development

The apparatus described here is not perfect but a work in progress and will benefit from further development by us and others. A substantial but not quantified fraction of the aerosols generated in the production or entrainment chamber is lost during transport, deposited on walls and tubing as evidenced by the surfaces of the apparatus darkening and acquiring a typical smell

35 for BrC depositions. Particle deposition onto the snow is not perfectly homogenous and this homogeneity varies from deposition to deposition. The dominant factor controlling homogeneity of the deposit seems to be wind, which causes the deposition to favor the lee side of the deposition area due to the air's ability to permeate and travel through the snowpack (Waddington et al., 1996). Additionally, this apparatus may alter the grain size of snow located at the top of the snowpack due to heating of the air inside the deposition volume. This could partly be mitigated by painting the deposition chamber white on

40 the outside to better reflect incident solar radiation. However, ensuring identical conditions inside and outside of the deposition chamber would be very challenging. Perhaps, the use of identical deposition chamber, one with and one without introduced aerosols could minimize this problem.

4 Conclusion and Discussion

The apparatus described here provides a means to generate or entrain and to artificially deposit aerosols evenly onto a snow surface. The apparatus has been proven to efficiently deposit carbonaceous aerosols – BC and BrC – from two combustion sources as well as entrained dry mineral dust onto snow, thereby altering the surface reflectivity of snow. The reduction of
5 spectral surface reflectivity was verified by measuring the directional surface reflectance within the area of deposition and comparing it to the reflectance of neighboring natural snow. The type of aerosol being deposited, and the total mass of that aerosol, can be adjusted by the users to suit their needs. Other applications of this apparatus could include the deposition of a wide variety of mineral dust from various regional dust entrainment areas as described by Engelbrecht et al. (2016). Another field of research opened up by this apparatus is testing of snow radiative transfer codes (e.g., SNICAR, TARTES, Flanner and
10 Zender, 2005; Libois et al., 2013) as to their treatment of the influence of impurities deposited onto the snowpack.

Data Availability. The authors provide the numerical values of HCRF spectra shown in figures within the manuscript in the supplementary material.

15 *Competing Interests.* The authors declare that they have no conflict of interest.

Acknowledgements. This material has been supported in part by NASA EPSCoR under Cooperative Agreement No. NNX14AN24A, NASA ROSES under Grant No. NNX15AI48G, and by the National Science Foundation under Grant No. AGS-1544425. It is a pleasure to acknowledge the Deep Sengupta for help with field experiments, Adam Watts for supplying
20 the peat samples, and Jeff Dozier and Mammoth Mountain Ski Resort for generously providing access to the CUES site.

References

Andreae, M. O. and Gelencsér, A.: Black carbon or brown carbon? The nature of light-absorbing carbonaceous aerosols, Atmos. Chem. Phys., 6(10), 3131–3148, doi:10.5194/acp-6-3131-2006, 2006.

Arnold, I. J., Berger, C., Chakrabarty, R. K., Moosmüller, H., Sharma, N. and Mazzoleni, C.: The iron lung: A device for the
25 continuous delivery of fine particulate matter, Rev. Sci. Instrum., 85(2), 25105, doi:10.1063/1.4865114, 2014.

Arnott, W. P., Moosmüller, H. and Walker, J. W.: Nitrogen dioxide and kerosene-flame soot calibration of photoacoustic instruments for measurement of light absorption by aerosols, Rev. Sci. Instrum., 71(12), 4545, doi:10.1063/1.1322585, 2000.

Bair, E. H., Dozier, J., Davis, R. E., Colee, M. T. and Claffey, K. J.: CUES—a study site for measuring snowpack energy
30 balance in the Sierra Nevada, Front. Earth Sci., 3, doi:10.3389/feart.2015.00058, 2015.

Bond, T. C. and Bergstrom, R. W.: Light absorption by carbonaceous particles: an investigative review, Aerosol Sci. Technol., 40(1), 27–67, doi:10.1080/02786820500421521, 2006.

Bond, T. C., Streets, D. G., Yarber, K. F., Nelson, S. M., Woo, J.-H. and Klimont, Z.: A technology-based global inventory of black and organic carbon emissions from combustion, J. Geophys. Res., 109(D14), D14203, doi:10.1029/2003JD003697,
35 2004.

Bond, T. C., Doherty, S. J., Fahey, D. W., Forster, P. M., Berntsen, T., DeAngelo, B. J., Flanner, M. G., Ghan, S., Kärcher, B., Koch, D., Kinne, S., Kondo, Y., Quinn, P. K., Sarofim, M. C., Schultz, M. G., Schulz, M., Venkataraman, C., Zhang, H., Zhang, S., Bellouin, N., Guttikunda, S. K., Hopke, P. K., Jacobson, M. Z., Kaiser, J. W., Klimont, Z., Lohmann, U., Schwarz, J. P., Shindell, D., Storelvmo, T., Warren, S. G. and Zender, C. S.: Bounding the role of black carbon in the
40 climate system: A scientific assessment, J. Geophys. Res. Atmos., 118(11), 5380–5552, doi:10.1002/jgrd.50171, 2013.

Brandt, R. E., Warren, S. G. and Clarke, A. D.: A controlled snowmaking experiment testing the relation between black carbon content and reduction of snow albedo, J. Geophys. Res., 116(D8), D08109, doi:10.1029/2010JD015330, 2011.

Cereceda-Balic, F., Vidal, V., Moosmüller, H. and Lapuerta, M.: Reduction of snow albedo from vehicle emissions at Portillo, Chile, Cold Reg. Sci. Technol., 146(November 2017), 43–52, doi:10.1016/j.coldregions.2017.11.008, 2018.

Chakrabarty, R. K., Moosmüller, H., Chen, L.-W. A., Lewis, K., Arnott, W. P., Mazzoleni, C., Dubey, M. K., Wold, C. E., Hao, W. M. and Kreidenweis, S. M.: Brown carbon in tar balls from smoldering biomass combustion, Atmos. Chem. Phys., 10(13), 6363–6370, doi:10.5194/acp-10-6363-2010, 2010.

Chakrabarty, R. K., Gyawali, M., Yatavelli, R. L. N., Pandey, A., Watts, A. C., Knue, J., Chen, L.-W. A., Pattison, R. R., Tsibart, A., Samburova, V. and Moosmüller, H.: Brown carbon aerosols from burning of boreal peatlands: microphysical properties, emission factors, and implications for direct radiative forcing, Atmos. Chem. Phys., 16(5), 3033–3040, doi:10.5194/acp-16-3033-2016, 2016.

Dang, C. and Hegg, D. A.: Quantifying light absorption by organic carbon in Western North American snow by serial chemical extractions, J. Geophys. Res. Atmos., 119(17), 10,247-10,261, doi:10.1002/2014JD022156, 2014.

Dozier, J.: Mountain hydrology, snow color, and the fourth paradigm, Eos, Trans. Am. Geophys. Union, 92(43), 373–374, doi:10.1029/2011EO430001, 2011.

Doherty, S. J., Warren, S. G., Grenfell, T. C., Clarke, A. D. and Brandt, R. E.: Light-absorbing impurities in Arctic snow, Atmos. Chem. Phys., 10(23), 11647–11680, doi:10.5194/acp-10-11647-2010, 2010.

Dubovik, O., Holben, B., Eck, T. F., Smirnov, A., Kaufman, Y. J., King, M. D., Tanré, D. and Slutsker, I.: Variability of absorption and optical properties of key aerosol types observed in worldwide locations, J. Atmos. Sci., 59(3), 590–608, doi:10.1175/1520-0469(2002)059<0590:VOAAOP>2.0.CO;2, 2002.

Engelbrecht, J. P., Moosmüller, H., Pincock, S., Jayanty, R. K. M., Lersch, T. and Casuccio, G.: Technical note: Mineralogical, chemical, morphological, and optical interrelationships of mineral dust re-suspensions, Atmos. Chem. Phys., 16(17), 10809–10830, doi:10.5194/acp-16-10809-2016, 2016.

Flanner, M. G. and Zender, C. S.: Snowpack radiative heating: Influence on Tibetan Plateau climate, Geophys. Res. Lett., 32(6), L06501, doi:10.1029/2004GL022076, 2005.

Flanner, M. G., Zender, C. S., Hess, P. G., Mahowald, N. M., Painter, T. H., Ramanathan, V. and Rasch, P. J.: Springtime warming and reduced snow cover from carbonaceous particles, Atmos. Chem. Phys., 9(7), 2481–2497, doi:10.5194/acp-9-2481-2009, 2009.

Gardner, A. S. and Sharp, M. J.: A review of snow and ice albedo and the development of a new physically based broadband albedo parameterization, J. Geophys. Res. Earth Surf., 115(1), 1–15, doi:10.1029/2009JF001444, 2010.

Grannas, A. M., Jones, A. E., Dibb, J., Ammann, M., Anastasio, C., Beine, H. J., Bergin, M., Bottenheim, J., Boxe, C. S., Carver, G., Chen, G., Crawford, J. H., Domine, F., Frey, M. M., Guzman, M. I., Heard, D. E., Helmig, D., Hoffmann, M. R., Honrath, R. E., Huey, L. G., Hutterli, M., Jacobi, H. W., Klan, P., Lefer, B., McConnell, J., Plane, J., Sander, R., Savarino, J., Shepson, P. B., Simpson, W. R., Sodeau, J. R., von Glasow, R., Weller, R., Wolff, E. W. and Zhu, T.: An overview of snow photochemistry: evidence, mechanisms and impacts, Atmos. Chem. Phys, 7(16), 4329–4373, doi:10.5194/acpd-7-4165-2007, 2007.

Hadley, O. L. and Kirchstetter, T. W.: Black-carbon reduction of snow albedo, Nat. Clim. Chang., 2(6), 437–440, doi:10.1038/nclimate1433, 2012.

Hegg, D. A., Warren, S. G., Grenfell, T. C., Doherty, S. J., Larson, T. V. and Clarke, A. D.: Source attribution of black carbon in Arctic snow, Environ. Sci. Technol., 43(11), 4016–4021, doi:10.1021/es803623f, 2009.

Hegg, D. A., Warren, S. G., Grenfell, T. C., Doherty, S. J. and Clarke, A. D.: Sources of light-absorbing aerosol in arctic snow and their seasonal variation, Atmos. Chem. Phys., 10(22), 10923–10938, doi:10.5194/acp-10-10923-2010, 2010.

Hodson, A., Anesio, A. M., Tranter, M., Fountain, A., Osborn, M., Priscu, J., Laybourn-Parry, J. and Sattler, B.: Glacial ecosystems, Ecol. Monogr., 78(1), 41–67, doi:10.1890/07-0187.1, 2008.

IPCC, 2013: Climate Change 2013: The Physical Science Basis. Contribution of Working Group I to the Fifth Assessment Report of the Intergovernmental Panel on Climate Change, edited by T. F. Stocker, D. Qin, G.-K. Plattner, M. Tignor, S. K. Allen, J. Boschung, A. Nauels, Y. Xia, V. Bex, and P. M. Midgley, Cambridge University Press, Cambridge, United Kingdom and New York, NY, USA., 2013.

Jacobson, M. Z.: Strong radiative heating due to the mixing state of black carbon in atmospheric aerosols., Nature, 409(6821), 695–7, doi:10.1038/35055518, 2001.

Jensen, W. B.: The Origins of the Hirsch and Büchner vacuum filtration funnels, J. Chem. Educ., 83(9), 1283, doi:10.1021/ed083p1283, 2006.

Jimenez, J. L., Canagaratna, M. R., Donahue, N. M., Prevot, A. S. H., Zhang, Q., Kroll, J. H., DeCarlo, P. F., Allan, J. D., Coe, H., Ng, N. L., Aiken, A. C., Docherty, K. S., Ulbrich, I. M., Grieshop, A. P., Robinson, A. L., Duplissy, J., Smith, J. D.,

Wilson, K. R., Lanz, V. A., Hueglin, C., Sun, Y. L., Tian, J., Laaksonen, A., Raatikainen, T., Rautiainen, J., Vaattovaara, P., Ehn, M., Kulmala, M., Tomlinson, J. M., Collins, D. R., Cubison, M. J., Dunlea, J., Huffman, J. A., Onasch, T. B., Alfarra, M. R., Williams, P. I., Bower, K., Kondo, Y., Schneider, J., Drewnick, F., Borrmann, S., Weimer, S., Demerjian, K., Salcedo, D., Cottrell, L., Griffin, R., Takami, A., Miyoshi, T., Hatakeyama, S., Shimono, A., Sun, J. Y., Zhang, Y. M., Dzepina, K., Kimmel, J. R., Sueper, D., Jayne, J. T., Herndon, S. C., Trimborn, A. M., Williams, L. R., Wood, E. C., Middlebrook, A. M., Kolb, C. E., Baltensperger, U. and Worsnop, D. R.: Evolution of Organic Aerosols in the Atmosphere, Science (80-.)., 326(5959), 1525–1529, doi:10.1126/science.1180353, 2009.

Jones, H. G.: The ecology of snow-covered systems: a brief overview of nutrient cycling and life in the cold, Hydrol. Process., 13(1415), 2135–2147, doi:10.1002/(SICI)1099-1085(199910)13:14/15<2135::AID-HYP862>3.3.CO;2-P, 1999.

Kuhn, M.: The nutrient cycle through snow and ice, a review, Aquat. Sci., 63(2), 150–167, doi:10.1007/PL00001348, 2001.

Lack, D. A., Moosmüller, H., McMeeking, G. R., Chakrabarty, R. K. and Baumgardner, D.: Characterizing elemental, equivalent black, and refractory black carbon aerosol particles: a review of techniques, their limitations and uncertainties., Anal. Bioanal. Chem., 406(1), 99–122, doi:10.1007/s00216-013-7402-3, 2014.

Laskin, A., Laskin, J. and Nizkorodov, S. A.: Chemistry of atmospheric brown carbon, Chem. Rev., 115(10), 4335–4382, doi:10.1021/cr5006167, 2015.

Libois, Q., Picard, G., France, J. L., Arnaud, L., Dumont, M., Carmagnola, C. M. and King, M. D.: Influence of grain shape on light penetration in snow, Cryosph., 7(6), 1803–1818, doi:10.5194/tc-7-1803-2013, 2013.

Lin, G., Penner, J. E., Flanner, M. G., Sillman, S., Xu, L. and Zhou, C.: Radiative forcing of organic aerosol in the atmosphere and on snow: Effects of SOA and brown carbon, J. Geophys. Res. Atmos., 119(12), 7453–7476, doi:10.1002/2013JD021186, 2014.

McConnell, J. R., Aristarain, A. J., Banta, J. R., Edwards, P. R. and Simões, J. C.: 20th-Century doubling in dust archived in an Antarctic Peninsula ice core parallels climate change and desertification in South America., Proc. Natl. Acad. Sci. U. S. A., 104(14), 5743–5748, doi:10.1073/pnas.0607657104, 2007.

Moosmüller, H., Chakrabarty, R. K. and Arnott, W. P.: Aerosol light absorption and its measurement: A review, J. Quant. Spectrosc. Radiat. Transf., 110(11), 844–878, doi:10.1016/j.jqsrt.2009.02.035, 2009.

Moosmüller, H., Chakrabarty, R. K., Ehlers, K. M. and Arnott, W. P.: Absorption Ångström coefficient, brown carbon, and aerosols: basic concepts, bulk matter, and spherical particles, Atmos. Chem. Phys., 11(3), 1217–1225, doi:10.5194/acp-11-1217-2011, 2011.

Moosmüller, H., Engelbrecht, J. P., Skiba, M., Frey, G., Chakrabarty, R. K. and Arnott, W. P.: Single scattering albedo of fine mineral dust aerosols controlled by iron concentration, J. Geophys. Res. Atmos., 117(D11), doi:10.1029/2011JD016909, 2012.

Painter, T. H., Barrett, A. P., Landry, C. C., Neff, J. C., Cassidy, M. P., Lawrence, C. R., McBride, K. E. and Farmer, G. L.: Impact of disturbed desert soils on duration of mountain snow cover, Geophys. Res. Lett., 34(12), L12502, doi:10.1029/2007GL030284, 2007.

Painter, T. H., Deems, J. S., Belnap, J., Hamlet, A. F., Landry, C. C. and Udall, B.: Response of Colorado River runoff to dust radiative forcing in snow, Proc. Natl. Acad. Sci., 107(40), 17125–17130, doi:10.1073/pnas.0913139107, 2010.

Painter, T. H., Skiles, S. M., Deems, J. S., Bryant, A. C. and Landry, C. C.: Dust radiative forcing in snow of the Upper Colorado River Basin: 1. A 6 year record of energy balance, radiation, and dust concentrations, Water Resour. Res., 48(7), doi:10.1029/2012WR011985, 2012.

Painter, T. H., McKenzie Skiles, S., Deems, J. S., Tyler Brandt, W. and Dozier, J.: Variation in rising limb of Colorado River snowmelt runoff hydrograph controlled by dust radiative forcing in snow, Geophys. Res. Lett., (February 2018), doi:10.1002/2017GL075826, 2017.

Patterson, E. M. and McMahon, C. K.: Absorption characteristics of forest fire particulate matter, Atmos. Environ., 18(11), 2541–2551, doi:10.1016/0004-6981(84)90027-1, 1984.

Peltoniemi, J. I., Gritsevich, M., Hakala, T., Dagsson-Waldhauserová, P., Arnalds, Ó., Anttila, K., Hannula, H.-R., Kivekäs, N., Lihavainen, H., Meinander, O., Svensson, J., Virkkula, A. and de Leeuw, G.: Soot on Snow experiment: bidirectional reflectance factor measurements of contaminated snow, Cryosph., 9(6), 2323–2337, doi:10.5194/tc-9-2323-2015, 2015.

Piedra, P. G., Llanza, L. R. and Moosmüller, H.: Optical losses of photovoltaic modules due to mineral dust deposition: Experimental measurements and theoretical modeling, Sol. Energy, 164(March), 160–173, doi:10.1016/j.solener.2018.02.030, 2018.

Qian, Y., Yasunari, T. J., Doherty, S. J., Flanner, M. G., Lau, W. K. M., Ming, J., Wang, H., Wang, M., Warren, S. G. and Zhang, R.: Light-absorbing particles in snow and ice: Measurement and modeling of climatic and hydrological impact, Adv. Atmos. Sci., 32(1), 64–91, doi:10.1007/s00376-014-0010-0, 2015.

Querry, M. R.: Optical Constants, Report No. AD-A158 623, Aberdeen Proving Ground, MD.

5 Reid, J. S., Koppmann, R., Eck, T. F. and Eleuterio, D. P.: A review of biomass burning emissions, part II: Intensive physical properties of biomass burning particles, Atmos. Chem. Phys. Discuss., 4(5), 5135–5200, doi:10.5194/acpd-4-5135-2004, 2004.

Samburova, V., Connolly, J., Gyawali, M., Yatavelli, R. L. N., Watts, A. C., Chakrabarty, R. K., Zielinska, B., Moosmüller, H. and Khlystov, A.: Polycyclic aromatic hydrocarbons in biomass-burning emissions and their contribution to light
10 absorption and aerosol toxicity, Sci. Total Environ., 568, 391–401, doi:10.1016/j.scitotenv.2016.06.026, 2016.

Schaepman-Strub, G., Schaepman, M. E., Painter, T. H., Dangel, S. and Martonchik, J. V.: Reflectance quantities in optical remote sensing—definitions and case studies, Remote Sens. Environ., 103(1), 27–42, doi:10.1016/j.rse.2006.03.002, 2006.

Seinfeld, J. H. and Pandis, S. N.: Atmospheric Chemistry and Physics: From Air Pollution to Climate Change, Third., John
15 Wiley & Sons, Inc., 2016.

Sengupta, D., Samburova, V., Bhattarai, C., Kirillova, E., Mazzoleni, L., Iaukea-lum, M., Watts, A., Moosmüller, H. and Khlystov, A.: Light absorption by polar and non-polar aerosol compounds from laboratory biomass combustion, (March), 1–45, doi:10.5194/acp-2018-161, 2018.

Singh, S. K., Kulkarni, A. V. and Chaudhary, B. S.: Hyperspectral analysis of snow reflectance to understand the effects of
20 contamination and grain size, Ann. Glaciol., 51(54), 83–88, doi:10.3189/172756410791386535, 2010.

Skiles, S. M., Painter, T. H., Deems, J. S., Bryant, A. C. and Landry, C. C.: Dust radiative forcing in snow of the Upper Colorado River Basin: 2. Interannual variability in radiative forcing and snowmelt rates, Water Resour. Res., 48(7), doi:10.1029/2012WR011986, 2012.

Skiles, S. M., Painter, T. and Okin, G. S.: A method to retrieve the spectral complex refractive index and single scattering
25 optical properties of dust deposited in mountain snow, J. Glaciol., 63(237), 133–147, doi:10.1017/jog.2016.126, 2017.

Sumlin, B. J., Pandey, A., Walker, M. J., Pattison, R. S., Williams, B. J. and Chakrabarty, R. K.: Atmospheric Photooxidation Diminishes Light Absorption by Primary Brown Carbon Aerosol from Biomass Burning, Environ. Sci. Technol. Lett., 4(12), 540–545, doi:10.1021/acs.estlett.7b00393, 2017.

Sumlin, B. J., Heinson, Y. W., Shetty, N., Pandey, A., Pattison, R. S., Baker, S., Hao, W. M. and Chakrabarty, R. K.: UV–
30 Vis–IR spectral complex refractive indices and optical properties of brown carbon aerosol from biomass burning, J. Quant. Spectrosc. Radiat. Transf., 206, 392–398, doi:10.1016/j.jqsrt.2017.12.009, 2018.

Thomas, W. H. and Duval, B.: Sierra Nevada, California, U.S.A., Snow algae: snow albedo changes, algal-bacterial interrelationships, and ultraviolet radiation effects, Arct. Alp. Res., 27(4), 389, doi:10.2307/1552032, 1995.

Warren, S. G.: Optical properties of snow, Rev. Geophys., 20(1), 67, doi:10.1029/RG020i001p00067, 1982.

35 Warren, S. G. and Wiscombe, W. J.: A Model for the spectral albedo of snow. II: snow containing atmospheric aerosols, J. Atmos. Sci., 37(12), 2734–2745, doi:10.1175/1520-0469(1980)037<2734:AMFTSA>2.0.CO;2, 1980.

Wu, G., Xu, T., Zhang, X., Zhang, C. and Yan, N.: The visible spectroscopy of iron oxide minerals in dust particles from ice cores on the Tibetan Plateau, Tellus B, 68, doi:10.3402/tellusb.v68.29191, 2016.

Zhang, X. L., Wu, G. J., Zhang, C. L., Xu, T. L. and Zhou, Q. Q.: What is the real role of iron oxides in the optical properties
40 of dust aerosols?, Atmos. Chem. Phys., 15(21), 12159–12177, doi:10.5194/acp-15-12159-2015, 2015.

Zhou, Y., Wang, X., Wu, X., Cong, Z., Wu, G. and Ji, M.: Quantifying light absorption of iron oxides and carbonaceous aerosol in seasonal snow across Northern China, Atmosphere (Basel)., 8(4), 63, doi:10.3390/atmos8040063, 2017.

Table 1: Overview of deposition and HCRF collection information

Site	Deposited Aerosol	Altitude (m)	Acquisition date	SZ* (°)	Avg. air temperature** (°C)
CUES, CA, USA	Hematite (Fe_2O_3)	2940	10 May 2016	24.5	8.4
Tamarack Lake, NV, USA	Brown carbon (BrC)	2694	02 May 2017	24.4	10.4
Tamarack Lake, NV, USA	Black Carbon (BC)	2694	24 April 2018	28.4	11.2

*   SZ: solar zenith angle at time of HCRF data collection
**   Average temperature during the HCRF data collection period. For the Tamarack Lake site, these values are taken
from the Mt Rose NRCS SNOTEL site, which lies 0.9 km southeast at 2683 m in altitude. For the CUES site, these are taken
5   directly from the CUES meteorological instrumentation.
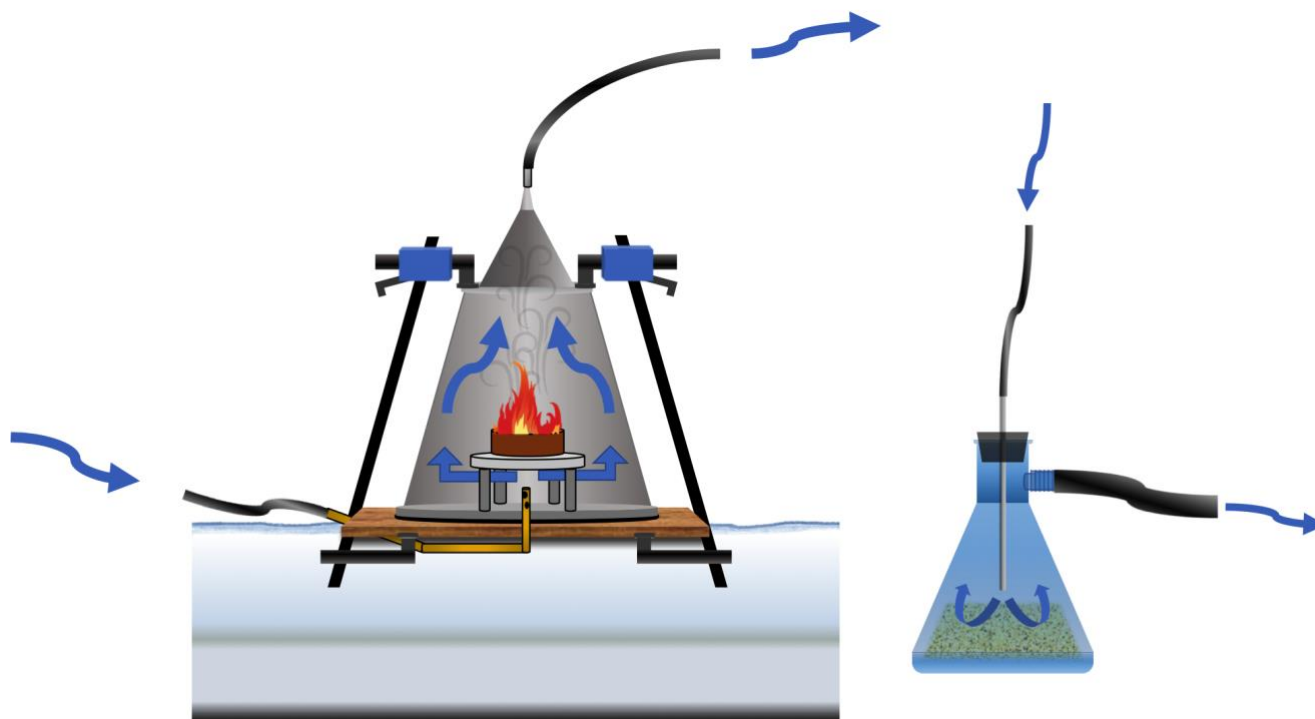
Figure 1: Schematic diagrams of the aerosol production and entrainment (right) chambers for producing combustion aerosol (left) and for dispersion of dry, pulverized dusts (right).

Figure 2: The deposition chamber for all aerosol types consists of a near cylindrical volume with aerosols pumped into the inlet at the top of the chamber from the production or entrainment chamber.

Figure 3: Use of the apparatus at the Tamarack Lake site for depositing BC aerosol.
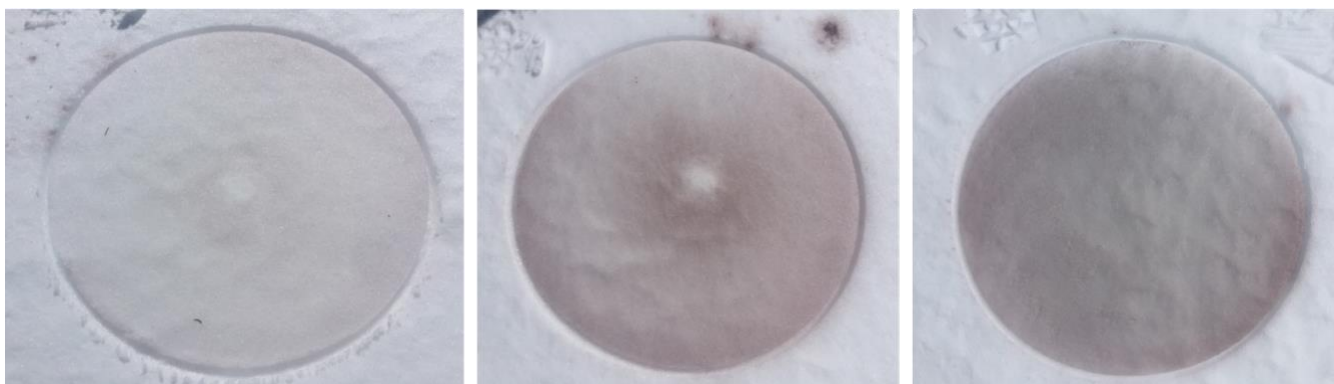
Figure 4: Images of three hematite depositions allow for visual inspection of the uniformity of the deposition.
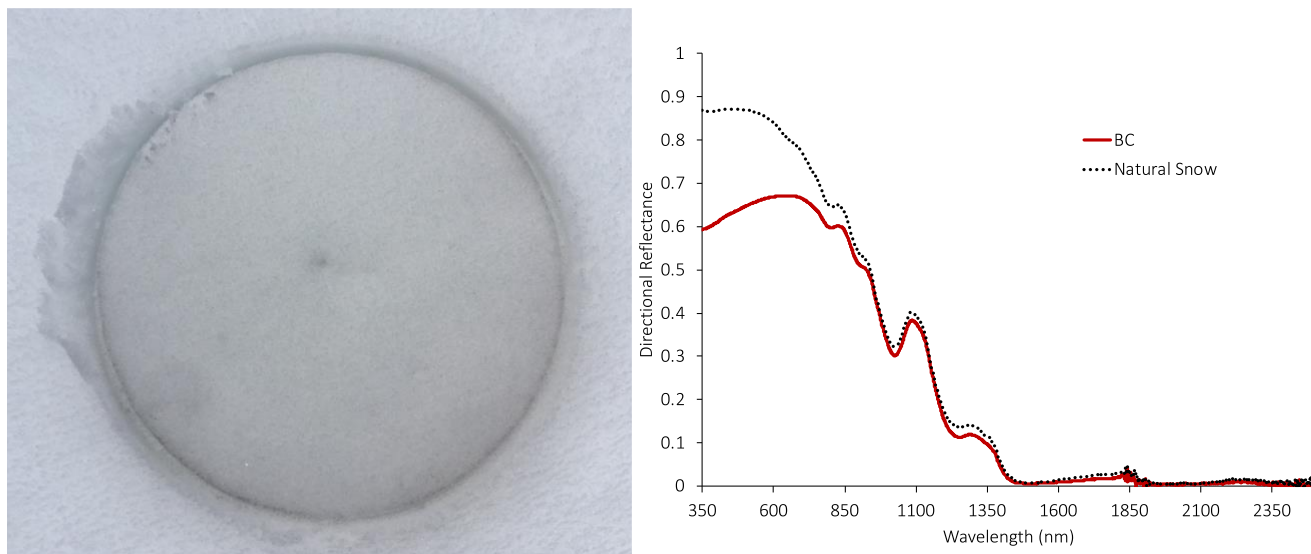
Figure 5: Image and HCRF spectra for a BC deposition and adjacent natural snow in May of 2018 at the Tamarack Lake site. This BC deposition drastically reduced the high natural snow reflectivity in the visible and near-visible spectral regions.
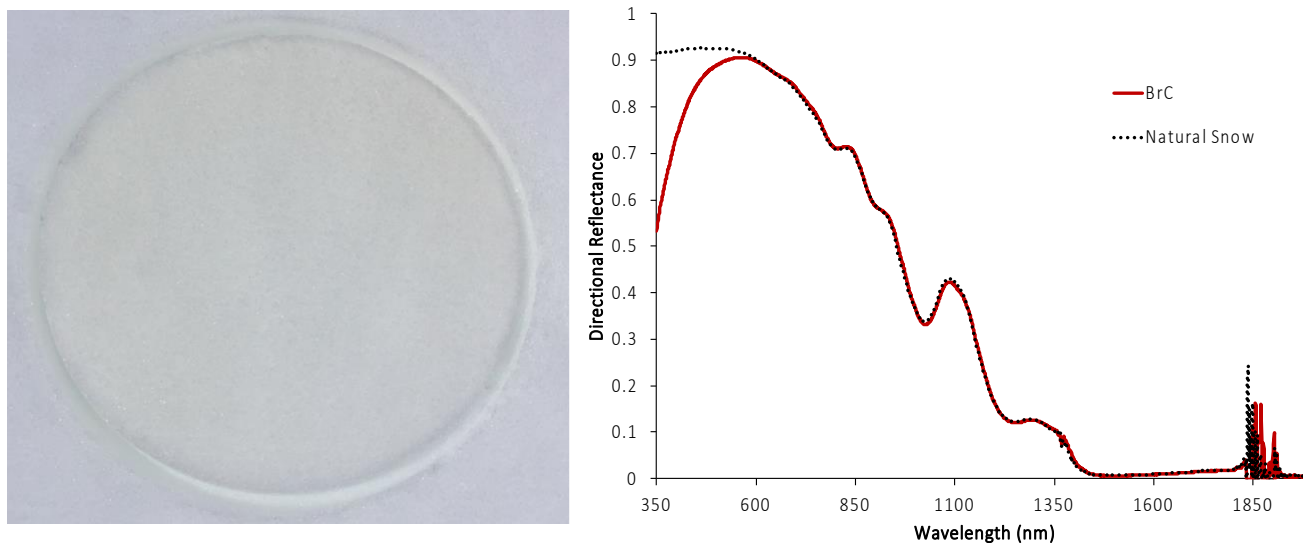
5   **Figure 6:** Image and HCRF spectra for a BrC deposition and adjacent natural snow in May of 2017 at the Tamarack Lake site. This BrC deposition drastically reduced the high natural snow reflectivity in the ultraviolet and short-wavelength visible (< 500 nm) spectral regions.
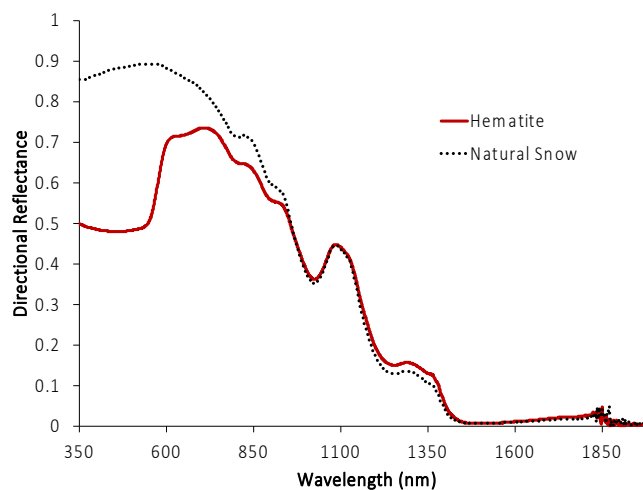
Figure 7: Image and HCRF spectra for a hematite deposition and adjacent natural snow in May of 2016 at the CUES research site. This hematite deposition drastically reduced the high natural snow reflectivity in the ultraviolet and short-wavelength visible (< 600 nm) spectral regions.